Influence of graphene oxide additives on the NF separation of triazine-based H_2S scavenging compounds using advanced membrane technology

Khalil, Alaa; Maschietti, Marco; Muff, Jens

Published in:
Chemosphere

DOI (link to publication from Publisher):
10.1016/j.chemosphere.2024.142439

Publication date:
2024

Document Version
Publisher's PDF, also known as Version of record

Chemosphere 360 (2024) 142439

Contents lists available at ScienceDirect

Chemosphere

journal homepage: www.elsevier.com/locate/chemosphere

Influence of graphene oxide additives on the NF separation of triazine-based H_2S scavenging compounds using advanced membrane technology

Alaa Khalil [a,b,*], Marco Maschietti [a], Jens Muff [a,b]

[a] Section of Chemical Science and Engineering, Department of Chemistry and Bioscience, Aalborg University, Niels Bohrs Vej 8, 6700, Esbjerg, Denmark
[b] Center for Membrane Technology, Aalborg University, Frederik Bajers Vej 7H, 9220, Aalborg Ø, Denmark

HIGHLIGHTS

- Novel TFN membranes incorporating graphene oxide (GO) were synthesized.
- The novel membranes were tested on spent and unspent H_2S scavenger wastewater.
- The inclusion of GO increases the permeability up to 26 times.
- The rejection of unspent MEA-triazine increases up to 80%.
- The selectivity of the separation unspent/spent scavenger is however decreased.

GRAPHICAL ABSTRACT

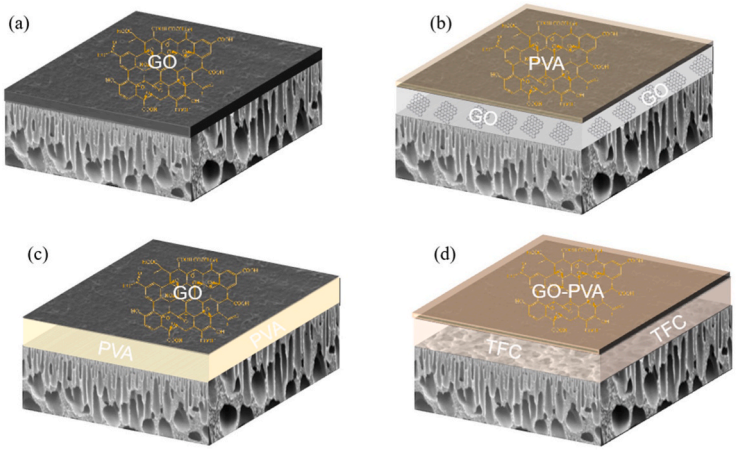

ARTICLE INFO

Handling Editor. Am Jang

Keywords:
Thin film nanocomposite
Graphene oxide
Antifouling
Interfacial polymerization
H_2S scavengers
MEA-Triazine

ABSTRACT

This work proposes an innovative approach for the membrane separation of spent and unspent H_2S scavengers (SUS) derived from the application of MEA-triazine in offshore oil and gas production. Modified nanofiltration membranes were fabricated by incorporating graphene oxide (GO) and polyvinyl alcohol (PVA) into a thin film composite (TFC) to obtain a thin film nanocomposite (TFN) with enhanced permeability. In addition, various immobilization strategies for GO were investigated. The performance of the membranes and the effect of the GO loading were evaluated in terms of permeability, fouling propensity, and rejection of key components of the SUS, i.e., MEA-triazine (unspent scavenger), dithiazine (spent scavenger), and monoethanolamine, operating on a sample of SUS wastewater obtained from an offshore oil and gas platform. Various characterization techniques, such as contact angle, FTIR, XRD, SEM, TGA, and AFM, were employed to evaluate the structure, composition, and hydrophilicity of the membrane. The results show a remarkable increase in permeability (from 0.22 Lm^{-2} h^{-1}

* Corresponding author. Section of Chemical Science and Engineering, Department of Chemistry and Bioscience, Aalborg University, Niels Bohrs Vej 8, 6700, Esbjerg, Denmark.
E-mail address: amaak@bio.aau.dk (A. Khalil).

https://doi.org/10.1016/j.chemosphere.2024.142439
Received 15 January 2024; Received in revised form 17 May 2024; Accepted 24 May 2024
Available online 24 May 2024

bar^{-1} for the TFC to 5.8 Lm^{-2} h^{-1} bar^{-1} for the TFN membranes), due to the enhanced hydrophilicity from GO incorporation. The strong interfacial interaction between GO and PVA within the TFN membrane results in negligible nanofiller leaching. The incorporation of GO moderately increases the rejection of the unspent scavenger (63%–73%, 62%–79%, 62%–80%, and 68%–76%), while drastically increasing the rejection of the spent scavenger, which is approximately null for the TFC membrane without GO and increases up to 58% in the TFN membrane with GO. Therefore, while the proposed membranes cannot be used for the selective separation of the unspent form the spent scavenger, they can achieve substantial recovery of all the key components contained in the SUS to avoid their discharge into the sea.

1. Introduction

Oil and gas operators face the challenge of removing hydrogen sulfide (H_2S) from produced fluids (gas, oil, and water). H_2S is a major impurity that causes corrosion of the infrastructure and poses health and safety issues due to its high toxicity. In offshore oil and gas installations H_2S is removed by injecting scavengers into the produced fluids. H_2S scavengers are chemicals that convert H_2S into components that are far less harmful and corrosive. With regard to natural gas, the content of H_2S in the export streams must be reduced to below approx. 4 ppm to comply with market specifications (Kelland, 2014). The most used H_2S scavenger consists of a basic aqueous solution of 1,3,5-tris(2-hydroxyethyl)-hexahydro-*s*-triazine (HET), also known as MEA-triazine. When injected into gas streams, it leads to the removal of H_2S by absorption and conversion into mainly monoethanolamine (MEA) and 5-(2-hydroxyethyl)hexahydro-1,3,5-dithiazine (DTZ), with the latter not having additional H_2S scavenging ability (Romero et al., 2023). Since MEA-triazine is typically used in large stoichiometric excess, the resulting aqueous phase contains both reaction products and unreacted MEA-triazine and it constitutes a distinctive wastewater stream (spent and unspent H_2S scavengers, henceforth called SUS), which is sometimes discharged into the sea without treatment due to the lack of feasible alternatives (Montesantos et al., 2022). When compared to the total produced water discharge from offshore oil and gas productions (e.g., 324 million m^3 per year in the North Sea (Karman and Smit, 2019)), SUS are very small streams. For example, it has been reported that the SUS in some North Sea installations account for less than 0.1% by volume of the total water discharge (Montesantos et al., 2023). Despite the small size, the discharge of unreacted MEA-triazine contained in the SUS was estimated to contribute to 20% of the environmental impact factor (EIF) of two North Sea fields (Stipanicev et al., 2018). This is due to the high concentration of water-soluble organic pollutants. Therefore, treating this small but concentrated streams, by preventing MEA-triazine and the scavenging reaction products to be discharged into the sea, can significantly reduce the EIF of offshore oil and gas production (Montesantos et al., 2023).

Membrane filtration is a cost-effective process for enhancing freshwater supply and for wastewater treatment. Notably, our previous studies have substantiated the potential of nanofiltration (NF) separation technology as a promising solution for treating SUS wastewater streams (Nikbakht Fini et al., 2021; Khalil et al., 2022a). Thin film composite (TFC) membranes, featuring an ultra-thin polyamide (PA) layer, a porous middle polysulfone (PSF) support layer, and a non-woven fabric base, have been widely used in nanofiltration (NF), forward osmosis (FO), and reverse osmosis (RO) due to their high selectivity, permeability, and energy efficiency (Cao et al., 2022; Wu et al., 2022). In one of our previous works, it was shown that a commercial NF270 membrane can separate MEA-triazine, which is the unspent scavenger, from DTZ, which is the spent scavenger (Nikbakht Fini et al., 2021). This outcome is significant from an environmental perspective as it shows a possible pathway for recovering unspent MEA-triazine, thus enabling the reduction of the chemical discharge into the marine ecosystem while offering economic advantages to operators via resource recovery and recycle. In a subsequent work, we developed a TFC membrane in house and focused on optimizing the filtration layer thickness. We successfully improved the recovery of the unspent MEA-triazine with higher membrane permeability compared to the commercial NF270 (Khalil et al., 2022a). However, TFC membranes are still subjected to a trade-off between permeability and rejection and require high operating pressures to achieve optimal pure water flux (Mansourpanah et al., 2021; Niu et al., 2022). For the perspective implementation of the membrane technology in offshore installations, it would be particularly desirable to further enhance the permeability of the membrane and to limit its fouling propensity, to allow the separation to be conducted in very small modules at low-pressure and with minimal maintenance.

Several strategies have been explored to improve the performance of TFC membranes. Surface modifications have been used to improve the porosity, cross-linking, pore structure, and hydrophilicity of the PA layer, which in turn improve the water permeability, selectivity, and antifouling ability (Butler et al., 2020). With regard to NF processes, considerable efforts have been made to improve the membranes. One strategy is to reduce the thickness of the selective PA layer to decrease the water transport resistance and to ensure optimal pore sizes for high rejection (Mokarizadeh et al., 2021). In addition, it is crucial to enhance the hydrophilicity and the surface roughness to increase the interaction between the water molecules and the membrane (Guo et al., 2019). However, it is difficult to simultaneously control the hydrophilicity, surface roughness, and thickness of the PA active layer without introducing defects. Another strategy is to incorporate hydrophilic nanomaterials into polymeric membranes through a mixed matrix process with a PA layer or into the mixed matrix membrane.

Among these methods, the incorporation of nanomaterials into the PA layer is a promising strategy for improving performance. Different types of nanomaterials, such as carbon-based materials, metal nanoparticles, metal organic frameworks, and metal oxide nanoparticles have been successfully incorporated into thin film nanocomposite (TFN) membranes (Zhao et al., 2018, 2023; Wang et al., 2022). The use of small amounts of these nanomaterials increases the surface roughness and the free volume of the selective layer, which in turn decreases the transport resistance and increases the hydrophilicity, resulting in improved performance of the modified TFN membrane (Wang et al., 2022). Among all kinds of nanomaterials, the incorporation of graphene oxide (GO) into polymeric membranes is a promising strategy to improve their performance. GO is a two-dimensional material composed of sp^2 carbon atoms with unique characteristics such as high mechanical strength, electrical/thermal conductivity, chemical stability, high surface area, and hydrophilicity (Izadmehr et al., 2020; Ng et al., 2020). It also possesses oxygen-containing functional groups on its surface, such as carboxyl, epoxy, and hydroxyl groups, which can enhance the hydrophilicity of the membrane and its resistance to fouling (Lai et al., 2018). In addition, the presence of GO in the PA layer can offer distinctive characteristics to the TFN membranes, providing a pathway for water molecules while blocking other substances through a combination of Donnan exclusion and steric hindrance, thus improving the water permeability, the rejection, and the antifouling performance (Poolachira and Velmurugan, 2022). In fact, recent studies have shown that the incorporation of GO into TFN membranes can improve their performance. For instance, Yin et al. (2016) prepared a TFN membrane with GO incorporated, and the results showed that increasing the

concentration of GO in a TFN membrane can lead to an increase in the permeate flux. Lai et al., 2016, 2018 discovered that incorporating GO into the TFN membranes can improve their hydrophilicity and surface negativity, resulting in improved water permeability and salt rejection. Bano et al. (2015) also found that incorporating GO into the structure of TFC membranes can improve their performance and antifouling properties. Han et al. (2013) prepared ultrathin graphene nanofiltration membranes by vacuum filtration of a suspension of reduced graphene oxide (rGO), which resulted in enhanced performance. However, these approaches face challenges related to the homogeneous distribution and long-term stability of the nanofillers within the membrane.

To overcome the challenges associated with the incorporation of nanofillers, we intend to utilize the adhesive property of polyvinyl alcohol (PVA) to develop a GO/PVA nanofiller-based layer on TFC membranes for SUS treatment application. PVA was used as an ideal adhesive for the incorporation of hydrophilic GO onto the membrane surface to improve the physicochemical properties of the membrane, such as surface chemistry, roughness, and charge, due to its highly adhesive properties and neutral charge (Ahmad et al., 2022; Lü et al., 2023). The synergistic compatibility between GO and PVA facilitated the formation of a uniform GO/PVA thin film, improving membrane performance and minimizing the leaching of nanofillers (Hung et al., 2019). In addition, PVA is recognized for its ability to enhance the hydrophilicity of membranes due to its hydroxyl groups, which can form hydrogen bonds with water molecules, thereby improving water transport and antifouling properties. These improvements are crucial for achieving superior TFN membrane performance in SUS treatment.

The aim of this work is to explore the effect of incorporating GO and PVA into TFC membranes on the separation of the water-soluble organics contained in the SUS. More specifically, it aims to determine whether the incorporation of GO and PVA can maintain the selective separation of spent and unspent components while increasing the permeability of the membrane. To achieve this goal, different strategies for incorporating GO and PVA into the membranes were also investigated. To the best of the authors' knowledge, no studies on the incorporation of GO in NF membranes for the separation of the SUS are reported in the literature. The performance of the membranes and the effect of GO loading were evaluated in terms of permeability, fouling propensity, and rejection of specific components operating on an offshore sample of SUS wastewater. Various characterization techniques such as contact angle, FTIR, XRD, SEM, TGA, and AFM, were used to evaluate the structure, composition, and hydrophilicity of the membrane.

2. Materials and methods

2.1. Materials

The PET non-woven support fabric (Novatexx 2413) was procured from Freudenberg Group (Germany). Polysulfone pellets (PSF), polyvinylpyrrolidone (PVP), polyvinyl alcohol (PVA), and *N*-methyl-2-pyrrolidone (NMP) were purchased from Sigma-Aldrich (Denmark). For the interfacial polymerization, *m*-Phenylenediamine (MPD, 99%), dopamine hydrochloride (DA), trimesoyl chloride (TMC, 98%), and n-hexane, (VWR, Redmond, WA) were utilized. Graphite powder was obtained from Graphit Kropfmühl GmbH. Sulfuric acid (H_2SO_4, 99%), phosphoric acid (H_3PO_4, 85%), potassium permanganate ($KMnO_4$, 99%), hydrogen peroxide (H_2O_2, 30%), hydrochloric acid (HCl, 37%), and nitric acid (HNO_3, 99%) were obtained from Sigma-Aldrich, Denmark. All reagents and solvents used were of analytical grade and required no additional processing.

The SUS solution was obtained from an offshore oil and gas production platform in the North Sea and stored at 4 °C. The SUS solution was analyzed for pH, conductivity, and viscosity, using a pH meter (Metrohm, 913), a conductometer (Metrohm, 912), and a cone and plate viscometer (Brookfield, CAP, 2000). The physical and chemical properties of the SUS solution are listed in Table S1 in the Supporting Information. External standards for the GC calibrations were prepared using 1,3,5-tris(2-hydroxyethyl)-hexahydro-*s*-triazine (HET, ≥95%, Santa Cruz Biotechnology), monoethanolamine (MEA, ≥99%, Acros Organics), and 5-(2-hydroxyethyl)hexahydro-1,3,5-dithiazine (DTZ, ≥98%, Toronto Research Chemicals). Methyl heptadecanoate (MHD, ≥99.0%, Sigma-Aldrich) and 1-Propanol (≥99.5%, VWR) were employed as internal standards for GC–MS and GC-FID, respectively, while dichloromethane (DCM, ≥99.8%, VWR) was utilized as solvent for liquid-liquid extraction.

2.2. Synthesis of GO

The synthesis of GO was based on Tour's method (Marcano et al., 2010). Briefly, a mixture of concentrated H_2SO_4 and H_3PO_4 (360:40 mL) was added to a mixture of graphite flakes (3.0 g) and $KMnO_4$ (18.0 g). After 12 h of heating and stirring at 50 °C, the mixture was cooled and slowly poured onto ice and 400 mL of water was slowly added. The reaction was terminated using 30% H_2O_2 (3 mL). The synthesis material was washed several times with water, HCl, and ethanol, and then dried overnight to obtain the final product.

2.3. Fabrication of GO-TFN membranes

The GO-TFN membranes were synthesized using the IP process, as schematically shown in Fig. S1. The process begins with drying the PSF powder; then, a mixture of PSF and PVP is added to NMP as a solvent and stirred overnight at 50 °C to obtain a homogeneous solution. The solution was cast on a PET nonwoven support using a film applicator (TQC Sheen, The Netherlands) with a casting knife with a gap of 100 μm and casting velocity of 5 mm/s, and immediately immersed in a coagulation bath for 24 h. The membranes were subsequently rinsed with deionized water (DI) and dried (Fig. S1a). Afterwards, the incorporation of GO was carried out by immersing the PSF membrane in a 2 wt% MPD aqueous solution and with different amounts of GO (0, 0.05, 0.10, 0.20 and 0.30 wt%) for 2 min, and then removing the excess solution (Fig. S1b). The membrane was then coated with 0.1 wt% TMC solution in n-hexane for 1 min (Fig. S1c), and the resulting GO-TFN membranes were washed, cured at 80 °C for 10 min, and stored in water (Fig. S1d). The prepared GO-TFN membranes were labeled based on the amount of GO: TFC, TFN0.05, TFN0.1, TFN0.2, and TFN0.3. In this approach, the MPD molecules in the aqueous solution adhered to the GO and participated in the reaction, resulting in the complete encapsulation of the GO within the formed PA layer. Furthermore, Fig. S2 illustrates various strategies for incorporating graphene oxide (GO) into the membrane. These strategies include the coating of the TFN membrane with PVA (PVA@TFN), embedding PVA within the PSF membrane and TFN membrane (TFN@PVA), and coating the TFC membrane with PVA-GO (GO-PVA@TFC).

2.4. Characterization

The surface and cross-sectional structure of the synthesized membranes were investigated using a scanning electron microscope (SEM, FEI Quanta 650F). The chemical composition was examined through Fourier transform infrared spectroscopy (FTIR, Thermo Scientific, Nicole iS5, US) and X-ray diffraction (XRD, Panalytical Ltd, Aeris, UK). The thermal stability was determined by thermogravimetric analysis using a TGA-550 equipment (TA Instruments, US) at a heating rate of 10 °C/min in N_2. The surface roughness of the TFN membranes was analyzed using an atomic force microscope (AFM, model MI5500, Agilent, USA). The membrane hydrophilicity was determined by measuring the contact angle of water droplets on the surface (KRÜSS DSA 100, Germany). The surface charge of the membrane was evaluated using an electrokinetic analyzer SurPASS (Anton Paar GmbH, Graz, Austria) and the effect of pH on the electrical charge was studied through automatic titration with

0.1 M HCl and 0.1 M NaOH.

2.5. Evaluation of performance and antifouling property

A cross-flow filtration unit (FT17-50, Armfield, UK) operating in semicontinuous mode, as shown in Fig. S3 in the Supporting Information, was employed to assess the performance of the membranes. Flat-sheet membrane disc samples were placed in a stainless-steel filtration cell with a diameter of 90 mm (effective filtration area of 63.6 cm^2), The system is pre-pressurized with deionized water for 1 h at a trans-membrane pressure (TMP) of 10 bar and 25 °C and the pure water flux is measured, before testing with the SUS. The feed was then switched to the SUS wastewater at zero-gauge pressure for 30 min to saturate the membrane surface (preconditioning). The experiments were conducted using 500 mL of SUS wastewater at a TMP of 10 bar and 40 °C, with a feed flow rate of 21 L/h and continuous recirculation of the retentate, a cross-flow velocity of 0.5 m/s and 50% permeate recovery (250 mL of permeate). To evaluate fouling, pure water flux was measured again after the filtration experiment at a TMP of 10 bar and 25 °C. In these experiments, a sample was taken from the feed after preconditioning, while the permeate was collected after the filtration (50% recovery), and the retentate was collected from the feed vessel at the end of the experiment (250 mL). All filtration runs were performed in duplicate. In addition, the fouling propensity of the synthesized membranes was further investigated in separate experiments by operating the membranes for at least 24 h under the same conditions using 1 L of SUS wastewater. The retentate and permeate were remixed and recirculated to the feed vessel. Samples of both the content of the feed vessel and the permeate were taken every 4 h to calculate the rejection of the SUS species and the permeability over time. The concentrations of HET and MEA were measured using a GC-FID method, while DTZ was measured by liquid-liquid extraction with DCM followed by GC-MS analysis. Each sample was analyzed three times with a relative standard deviation (RSD) less than 5% of the average value. The methods used for the measurements and the analysis have been described elsewhere (Nikbakht Fini et al., 2021).

The permeability of the membranes and the rejection of the SUS key species were calculated using the following equations:

$$P_m = \frac{V_P}{A\Delta Pt} \quad \text{Eq. 1}$$

$$R = 1 - \frac{C_P}{½(C_F + C_R)} \quad \text{Eq. 2}$$

where V_p is the permeate volume in a certain filtration time t, A is the effective filtration area, ΔP is the transmembrane pressure, and C_F, C_P, and C_R are the concentrations of the species under consideration in the feed, permeate and retentate, respectively.

2.6. Evaluation of leaching

The potential of GO to leach out from the membrane was investigated using a method described by Igbinigun et al. (2016). In this test, four membranes (TFN0.3, PVA@TFN0.3, TFN0.3@PVA, and 0.3GO-PVA@TFC) with a surface area of 19.64 cm^2 were individually submerged in a tube filled with 50 mL of DI water. The content of the tube was shaken for 5 days at room temperature by continuous rotation at 200 rpm. Water samples (3 mL) were taken every 24 h and the entire volume of water within the tube was replaced with fresh DI water after each sampling interval. The GO in the water samples was then quantified using a UV–vis spectrophotometer (Agilent Tech, Cary 60) operating at a wavelength of 245 nm. This quantity represents the amount of GO leached out from the membrane. A UV-calibration curve for quantifying GO was prepared, using solutions of GO in water at four concentration levels in the range 0–0.03 wt% and measuring each sample in duplicate. The R^2 value of the straight-line calibration curve was 0.9887, as depicted in Fig. S4 in the Supporting Information.

2.7. Determination of membrane porosity and mean pore size

The porosity of the fabricated membranes was measured using the gravimetric method. The membranes (with a surface area of 19.64 cm^2) were immersed in DI water for 48 h, removed from the water and weighed. Afterwards, the mass of the membrane samples was determined again after drying in an oven at 60 °C for 24 h. The porosity was then calculated using Eq. (3)

$$Porosity\ (\varepsilon) = \frac{M_w - M_d}{\rho_w A\delta} \quad \text{Eq. 3}$$

where M_w and M_d are the masses of the wet and dry membranes, respectively, ρ_w is the water density, A and δ are the surface area and the thickness of the membranes, respectively. Three measurements were performed for each sample. Based on water flux and porosity data, the average mean pore size of the membranes was calculated using the Guerout-Elford-Ferry equation reported in Eq. (4) (Khalil et al., 2022b):

$$Pore\ size\ (r_m) = \frac{\sqrt{(2.9 - 1.75\varepsilon) \bullet 8\eta\delta Q}}{\varepsilon A\Delta P} \quad \text{Eq. 4}$$

where η is the water viscosity at 25 °C, while Q and ΔP are the membrane permeate water flux and the transmembrane pressure, respectively.

3. Results and discussion

3.1. Membrane morphology

The surface morphology and cross-section of the synthesized membranes were examined using SEM as shown in Fig. 1. All TFN membranes exhibit a typical ridge-and-valley structure, resulting from the MPD, TMC, and GO interaction, and the hydrophilic group of GO, in line with the literature (Bano et al., 2015; Ma et al., 2018). In contrast, the TFC membrane displays a smoother surface (Khalil et al., 2022a). In addition, PVA coating on PA leads to a roughened morphology (Fig. 1b), which is consistent with previous studies (Zhang et al., 2016; Chong et al., 2019). This difference in roughness between TFN and PVA@TFN membranes is attributed to the wrinkled structure of GO (Cheng et al., 2019; Lai et al., 2019). Moreover, the increased surface roughness of TFN@PVA and GO-PVA@TFC membranes compared to the PVA@TFN membranes may be attributed to the random orientation of GO within the PVA matrix caused by hydrogen bonding between the functional groups of PVA and GO. Similar observations have been reported for GO-PVA composites (Dave and Nath, 2016).

The surface of the TFN and PVA@TFN membranes has a typical large leaf-like structure (ridge-and-valley) morphology, while the TFN@PVA and GO-PVA@TFC membranes have larger nodular structures on the PA layer surface. This difference in surface morphology is mainly due to the hydrophilicity and pore size of the PA layer (Ghosh and Hoek, 2009). The amine monomers in the MPD tend to interact with the polar functional groups of the hydrophilic substrate, which reduces the diffusion rate of the amine monomers from the pores to react with the acyl chloride monomers (Ghosh and Hoek, 2009). However, this theory may not apply to hydrophilic substrates with small pore sizes as the release of amine monomers from the coating layer may be restricted, reducing their ability to react with acyl chloride monomers (Shukla et al., 2017; Ng et al., 2020). This can lead to the formation of a thicker, rougher surface with larger nodules within the substrate pores, instead of on the membrane surface. The combination of enhanced hydrophilicity and decreased substrate pore size, as discussed later, results in the development of a thin and nodular PA structure as observed on the TFN membranes. However, introducing GO into the interlayer can enhance the hydrophilicity and reduce the pore size, allowing amine monomers

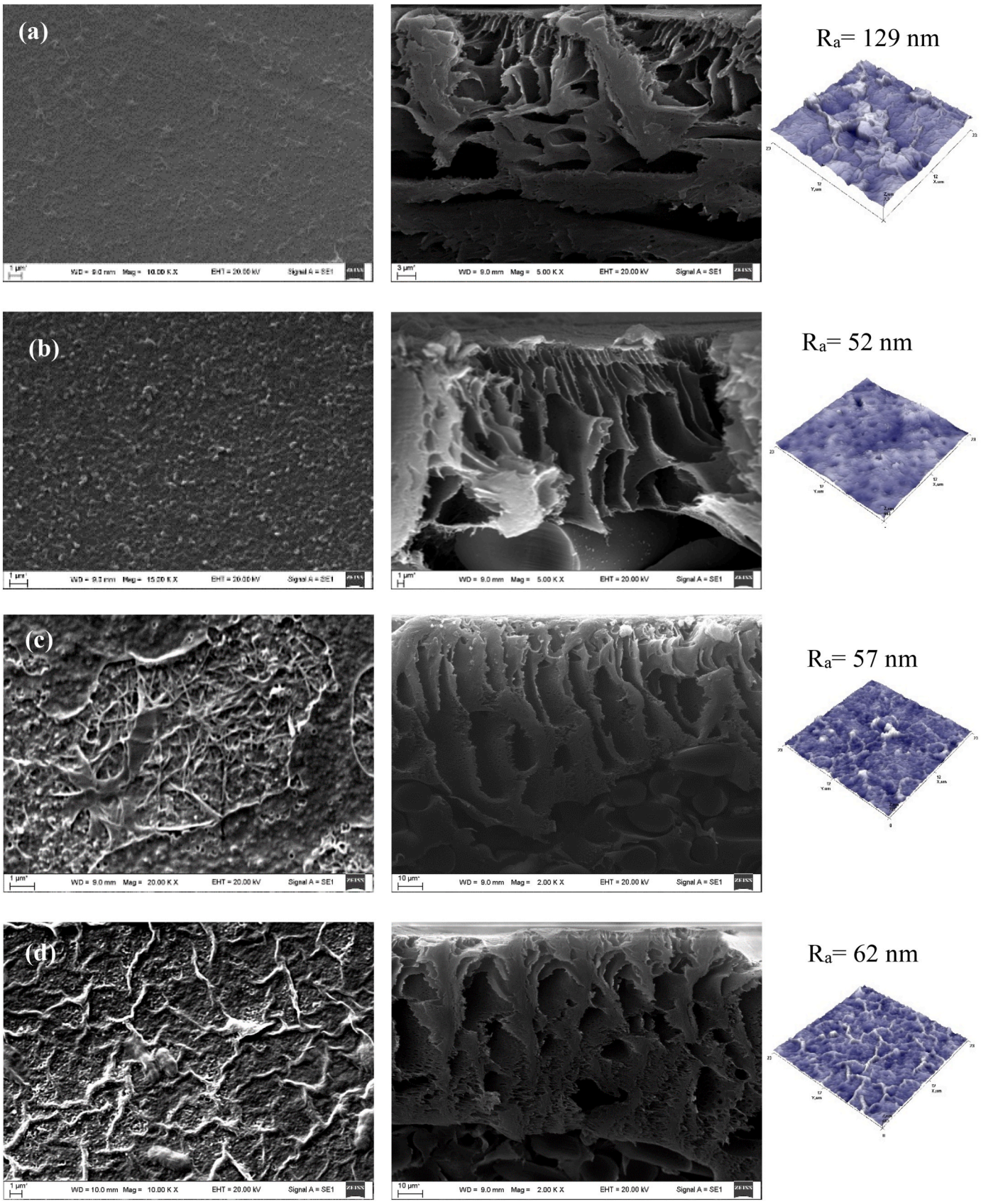

Fig. 1. SEM images of surface morphology, cross-sectional images, and AFM images of the prepared membranes: a) TFN0.2, b) PVA@TFN0.2, c), TFN0.2@ PVA, and d) 0.2GO-PVA@TFC.

to remain at the substrate surface and react with TMC (Xue et al., 2016). This results in the formation of a thicker composite layer with a larger leaf-like structure, as shown in the TFN@PVA and GO-PVA@TFC (Fig. 1c and d). Similar results were observed when hydrophilic halloysite nanotubes were added to the polydopamine interlayer of TFN membranes for forward osmosis applications (Shah et al., 2019).

To further investigate the structural changes in the synthesized membranes, the cross-sectional morphologies of the TFN, PVA@TFN, TFN@PVA, and GO-PVA@TFC membranes were examined and the results are shown in Fig. 1. The cross-sectional SEM images show that all the synthesized membranes exhibit an asymmetric structure with a dense top layer and a porous sublayer with uniform and long finger-like macro-voids. A thin PA layer has formed over the surface of the PSF membrane, and all the prepared membranes have a thin PA layer with an average thickness of 100–220 nm. In addition, the AFM images (Fig. 1) show that the surface roughness of the PA layer is reduced. This behavior is due to the addition of PVA into the aqueous solution and the formation of hydrogen bonding between GO and PA during the IP process, which enhances the hydrophilicity, water flux, and fouling resistance of the membranes, which is consistent with previous literature findings (Ugur Nigiz, 2020; Amiri et al., 2023). However, the TFN membrane shows a higher roughness, which may be due to the agglomeration of GO at higher loadings.

3.2. Membrane surface chemistry

Fig. 2 presents the FTIR spectra of the fabricated nanocomposite membranes at 0.2 wt% of GO loading. The presence of characteristic peaks at 1585 cm^{-1} (C–N stretching) and 1670 cm^{-1} (C]O stretching vibration of amide I) on all the membranes indicates the successful formation of the PA layer during the interfacial polymerization (Ng et al., 2020). Meanwhile, the broad peak around 3460–3000 cm^{-1}, corresponding to C–H and O–H stretching vibrations, confirms the presence of hydrophilic groups on the GO surface (Chong et al., 2019). The minimal difference in the spectra of the TFC and TFN membranes is attributed to the very low amount of nanofillers used during their fabrication, which aligns with the findings reported by Miao et al. (Wu et al., 2021). Furthermore, peaks at 1494 cm^{-1}, 1238 cm^{-1}, 1148 cm^{-1}, and 830 cm^{-1} were observed in the PSF for aromatic C]C, asymmetric C–O–C, symmetric O]S]O stretching, and C–H stretching, respectively (Khalil et al., 2022a).

Fig. 3a presents the XRD patterns of the nanocomposite membranes used to investigate their crystallinity. The results show that all TFN membranes display three distinct diffraction peaks at 2θ values of 17.65°, 22.81°, and 25.87°, corresponding to the (010), (110), and (100) planes, respectively. These results confirm the semi-crystalline structure of the TFN membranes. The thermal stability is presented in Fig. 3b, which shows the thermal gravimetric analysis (TGA) curves of the TFN membrane. As can be seen, there are four main stages of weight loss, which are represented by three peaks in the differential thermogravimetric (DTG) curves. The first stage, which occurs between 85 and 180 °C (Tp,1 at 160 °C), is attributed to water evaporation and associated to a weight loss of 1.5 wt%. The second stage, between 345 and 450 °C (Tp,2 at 427 °C), accounts for 60.3% of the weight loss and is attributed to the thermal decomposition of the PET substrate. The third stage, around 450–520 °C (Tp,3 at 504 °C), is due to the degradation of the PA layer and is associated to a weight loss of 14.2%. Finally, the fourth stage, beginning at 525 °C, is associated to the complete degradation of the membrane, resulting in a total weight loss of about 79.4 wt % at 700 °C. The results indicate that the thermal stability of the membranes is enhanced by incorporating GO into the PA layer due to the strong interfacial bonding between the polar functional groups in GO and the PA layer.

3.3. Membrane surface hydrophilicity

Water contact angle is a crucial indicator of membrane surface wettability and hydrophilicity. The water contact angle of each membrane was measured using the sessile drop technique at various points. Various spots on each membrane type were measured, and the results are displayed in Fig. 4, with error bars representing standard deviations. The results indicate a decreasing trend in contact angle with increasing GO loading (Fig. 4a). The TFN0.3 membrane displays the lowest water contact angle of 23°, while the TFC membrane has the highest water contact angle of 51°. This trend is attributed to the hydrophilic nature of GO carboxylic groups and the enhanced membrane roughness, consistently with previous findings (Huang et al., 2016; Lai et al., 2018). In addition, the GO functional groups promote the crosslinking of the PA layer that further improves the surface wettability of the membranes, which is consistent with previous studies (Idris et al., 2020). Furthermore, Fig. 4b shows the hydrophilicity of the synthesized membranes using different synthesis strategies. All the prepared membranes exhibited higher hydrophilicity than the TFC membrane. Notably, the PVA@TFN and GO-PVA@TFC membranes exhibit lower contact angle than the TFN membrane due to the presence of exposed –OH groups on the PVA surface. The incorporation of GO leads to a decrease in the water contact angle, indicating an increased hydrophilicity of the membrane surface. This is attributed to the oxygen domain of GO and to the non-crosslinked hydroxyl group of PVA. The improved hydrophilicity is expected to enhance the antifouling properties and permeability of the TFN membrane during the wastewater filtration.

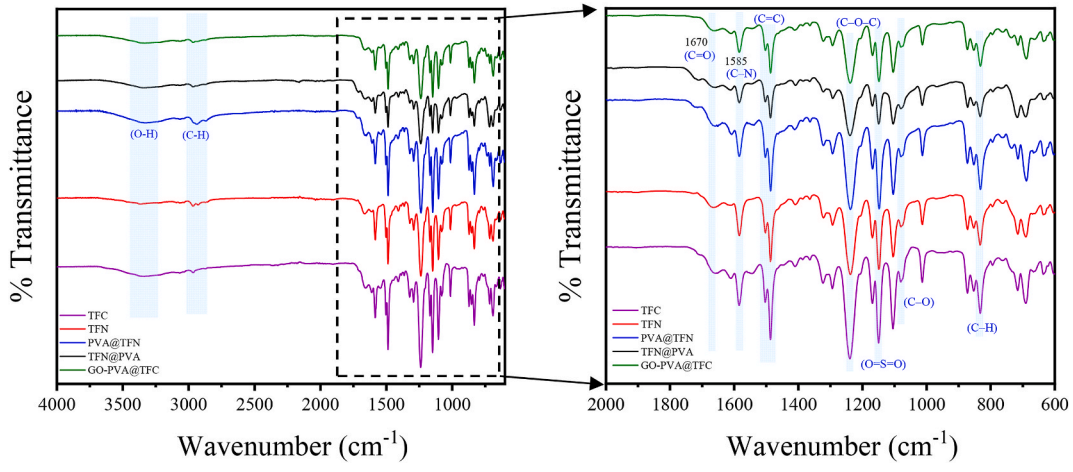

Fig. 2. FTIR spectra of the fabricated membranes.

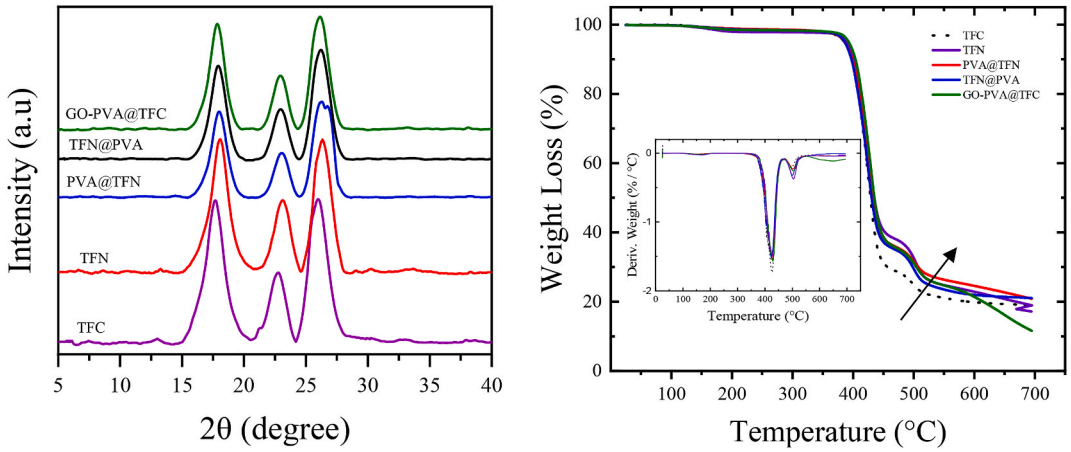

Fig. 3. XRD and TGA of the fabricated membranes.

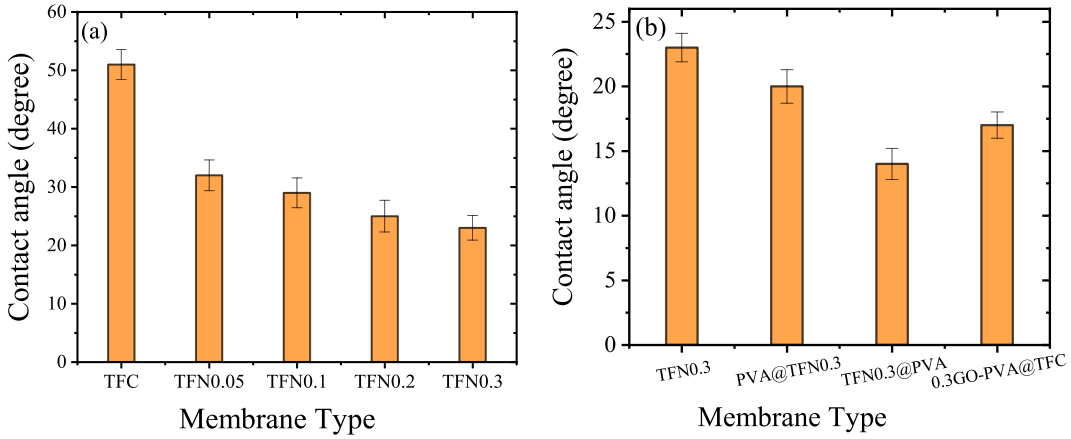

Fig. 4. Water contact angle of (a) TFN, and (b) prepared membranes at 0.3 wt % of GO loading.

3.4. Nanofiller leaching

Measuring the leaching of nanofillers is important to evaluate the stability of the membranes, ensuring that the nanofillers do not migrate from the membranes into the surrounding environment. The results of the nanofiller leaching tests, shown in Fig. S5 in the Supporting Information, indicate minimal leaching of GO, with the highest amount observed on Day 1 followed by Day 2, and no more GO detected after Day 2. The total amount of GO leaching throughout the agitation period is negligible, with values of only 25, 5.1, 25, 2.2, and 14.4 μg/g for the TFN, PVA@TFN, TFN@PVA, and GO-PVA@TFC membranes, respectively. The initial leaching on the first two days can be attributed to loosely attached GO. The results confirm that the formed layers have good stability due to the strong interaction between GO and PVA through intermolecular H-bonding and the crosslinking of PVA with GA, which minimizes the loss of GO in the long run, in agreement with previous results (Kashyap et al., 2016). These results confirm that the process for preparing TFN membranes is possible and any leaching of the GO does not have a significant impact on the quality of the retentate and permeate as the microporous substrate can effectively capture the flake-shaped GO (Lai et al., 2019).

3.5. Porosity and mean pore sizes of the synthesized membranes

The evaluation of the mean pore size and porosity is crucial for understanding the rejection and permeability characteristics of the membrane. Fig. 5 displays the porosity and the mean pore size of the synthesized membranes. For each membrane, three measurements were performed at a GO loading of 0.3 wt% and the error bars indicate the standard deviations. The results show that the TFN0.3@PVA membrane has the highest porosity, while the TFN0.3 membrane has the lowest porosity. In addition, the mean pore size was calculated using Eq (4) for all the fabricated membranes, and it was found that the 0.3GO-PVA@TFC membranes have the highest mean pore size. TFN0.3, PVA@TFN0.3, TFN0.3@PVA, and 0.3GO-PVA@TFC membranes have a

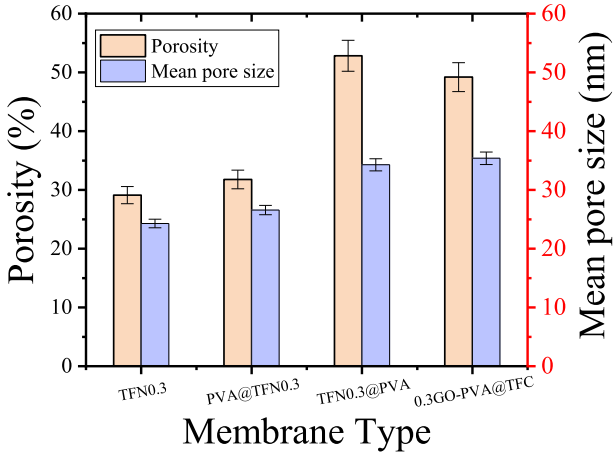

Fig. 5. Porosity and mean pore size for synthesized membranes at 0.3 wt % of GO loading.

mean pore size of 24, 27, 34, and 35 nm, respectively. The larger mean pore sizes of the TFN0.3@PVA and 0.3GO-PVA@TFC membranes can be attributed to the enhanced mass transfer rate between the solvent and non-solvent phases during the phase inversion process (Wang et al., 2012). It is worth noting that the TFN0.3 membranes were selected for testing the water contact angle, nanofiller leaching, pore size, and porosity to demonstrate the influence of GO on the structural and surface properties of the membranes at the highest loading, where its effects are more pronounced.

3.6. Separation performance of the TFN membrane

The permeability and the rejection of individual chemical species of the TFC and TFN membranes were evaluated on the SUS wastewater and the results are shown in Fig. 6. The incorporation of GO nanoparticles into the filtration layer results in a significant enhancement in permeability compared to the TFC membrane, which is in line with expectations from the literature (Kang et al., 2019). The permeability increased with a factor of 15, from 0.22 to 3.4 $Lm^{-2}h^{-1}$ bar^{-1}, when the GO loading was increased from 0 to 0.1 wt%, before slightly decreasing to 2.2 $Lm^{-2}h^{-1}$ bar^{-1} at 0.3 wt%. The enhanced permeability is explained in the literature by a rougher and more hydrophilic surface promoting water adsorption and the formation of additional water passages between the PA chains and the GO nanoparticles, which enhances the water transfer rates through the hydrophilic structure of the PA layer (Amini et al., 2013; Kong et al., 2020). The internal voids within the GO particles may also contribute to the improved permeability (Khoo et al., 2022). The slight decrease in permeability at higher GO loadings may be associated with GO agglomeration causing non-uniform distribution in the filtration layer preventing full utilization (Ge et al., 2023).

Regarding the rejection of individual chemical species, HET, MEA and DTZ are affected in different ways by the incorporation of GO. As can be seen in Fig. 6, the TFC membrane shows a 58% rejection of HET, which increases slightly for GO additions up to 0.2 wt%, where the rejection reaches 74%. The difference in rejection of HET between GO 0.2 and 0.3 wt% does not appear to be significative, due to a large overlap of the duplicate test error bars. As for MEA, no trend is observed, and the calculated rejections are in the range of 35%–47% for all membranes. The most notable observation is the substantial rejection of DTZ caused by the incorporation of GO, even at the initial loading of 0.05 wt%. Compared to the TFC membrane, DTZ rejection increases from 1% to 57% at 0.05 wt% and it stays approximately constant up to 0.2 wt% before a decrease in rejection to 30% is observed at a 0.3 wt% GO loading.

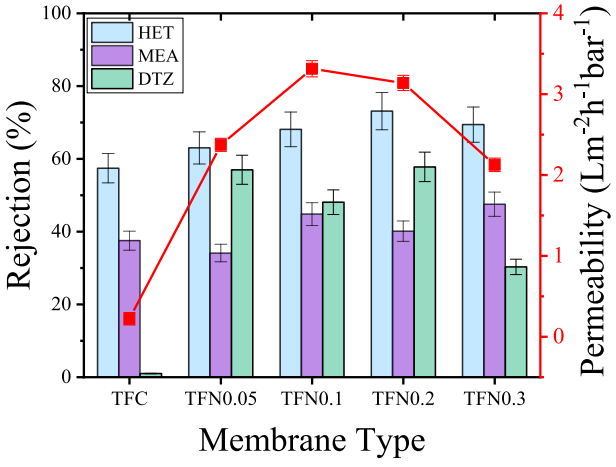

Fig. 6. Rejection of HET, MEA and DTZ and permeability of the fabricated TFN membranes at varying GO loading (measured at permeate recovery of 50 %). The error bars represent the standard deviations for duplicate experiments.

This change in membrane selectivity from a TFC membrane, with some rejection of HET and MEA but almost no rejection of DTZ, to a TFN membrane, with rejection of DTZ as well, is caused by the GO addition and it is an unexpected finding. DTZ is a polar molecule (the dipole moment is provided in the Supporting Information in Table S2) and a reason for the changed behavior may be ascribed to stronger dipole-dipole intermolecular adsorption forces between DTZ and the membrane surface caused by the hydrophilic functionalized GO particles, thus reducing the transport of DTZ through the membrane (Nikbakht Fini et al., 2021). For the TFN membranes it is also seen that, for GO up to 0.2 wt%, the rejection of the larger solutes (HET and DTZ) is higher than that of the smaller solute MEA, which is in contrast with the TFC membrane and may indicate that size exclusion plays a larger role in membranes with the incorporation of GO.

GO loaded TFN membranes were synthesized using different strategies and at different loadings, and their filtration performance was compared to TFC as shown in Fig. S6 in the Supporting Information. The results show that the permeability of the prepared membranes is mainly affected by the loading of GO. The TFN0.2@PVA membrane exhibits higher HET rejection (80%) than the TFN0.2 (74%), PVA@TFN0.2 (79%), and 0.2GO-PVA@TFC (68%) membranes. The rejection capabilities of the PVA@TFN0.1, PVA@TFN0.2, and PVA@TFN0.3 membranes for HET, DTZ, and MEA show negligible changes after PVA coating. Moreover, TFN@PVA membranes exhibit higher permeability (5.9 $Lm^{-2}h^{-1}$ bar^{-1}) among the tested membranes. The lower permeability of the TFN and PVA@TFN membranes can be explained by surface defects in the PA layer caused by the larger amount of GO, making it challenging for the thin PA layer to completely cover the GO nanoparticles (Yin et al., 2016). On the other hand, the TFN@PVA membranes exhibit a remarkable 175% increase in permeability compared to the TFN membranes. This increase in permeability is probably due to the enhanced membrane hydrophilicity and increased surface roughness resulting from PVA and GO incorporation (Ali et al., 2016; Dave and Nath, 2016). In addition, the pure water flux across different membrane types before and after filtration is shown in Fig. S7 in the Supporting Information. TFN0.1 and TFN0.2 exhibit the highest pure water flux and show minimal flux decline after filtration, indicating better resistance to fouling.

3.7. Long-term stability and fouling propensity of the TFN membrane

Membrane fouling is a significant concern as it can lead to a reduction in the permeability and the membrane lifespan. Therefore, the evaluation of membrane fouling properties is important. The operational stability of TFN membranes is a critical aspect for their successful commercial implementation. To assess the performance stability and antifouling property of the TFN membrane, a long-term test was conducted to measure the rejection of SUS key compounds and the membrane permeability over 24 h as shown in Fig. 7. The TFN0.2 membrane was selected for this experiment since it showed the highest rejection factor for HET. The results reveal a consistent and stable performance of the TFN membrane, with minimal changes in permeability and rejection of compounds, as well as no significant decrease in flux during the 24 h testing period.

In summary, compared to the virgin TFC membranes, the developed TFN membranes, with incorporation of GO in the filtration layer, increase the average permeability with a factor of up to 15 but on the cost of the loss of the selective separation of the unspent (HET) from the spent H_2S scavenger (DTZ).

4. Conclusions

The incorporation of graphene oxide (GO) and polyvinyl alcohol (PVA) in Thin Film Composite (TFC) membranes leads to a substantial increase of permeability with respect to spent and unspent H_2S scavengers (SUS). The permeability increases from 0.22 Lm^{-2} h^{-1} bar^{-1} for

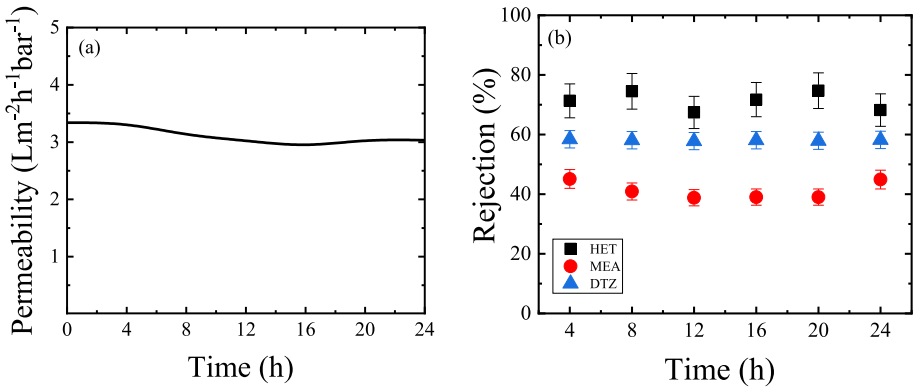

Fig. 7. Long-term stability of TFN0.2 membrane: a) Filtration permeability and b) HET, MEA, and DTZ rejection during 24 h continuous filtration at 40 °C.

the TFC membrane without GO, up to 5.8 $Lm^{-2} h^{-1} bar^{-1}$ for a Thin Film Nanocomposite (TFN) membrane with 0.1 wt% GO. The permeability is approximately constant in the range 0.1 wt% to 0.2 wt% GO, while decreasing at higher GO loading. The increased permeability of the TFN membranes, compared to the TFC, is attributed to the increased membrane hydrophilicity caused by the incorporation of GO. The inclusion of polyvinyl alcohol (PVA) is effective in stabilizing the nanofiller, while having no substantial effect on the permeability, whose increase is caused by the incorporation of GO. Furthermore, the permeability is kept approximately constant in 24 h of operation, indicating no sign of quick onset of fouling issues.

While the TFN membrane shows a slight improvement in the rejection of MEA-triazine (the unspent scavenger), the inclusion of GO and PVA significantly increases the rejection of dithiazine (the spent scavenger), which is instead negligible in the TFC membranes without GO. Therefore, the TFN membranes do not selectively separate MEA-triazine from dithiazine and cannot be used for the purpose of the selective recovery of the unspent scavenger form the SUS. On the other hand, since they exhibit good rejections towards all key organic species in the SUS wastewater (MEA-triazine, dithiazine, and monoethanolamine) they could be used for the recovery of most of the organics contained in the SUS to clean the wastewater before the discharge into the sea. This approach would contribute to concentrating the organic pollutants into a smaller stream, potentially facilitating easier on-site (offshore) processing or shipping small volumes of waste to onshore for processing.

CRediT authorship contribution statement

Alaa Khalil: Writing – review & editing, Writing – original draft, Visualization, Validation, Software, Resources, Methodology, Investigation, Formal analysis, Data curation, Conceptualization. **Marco Maschietti:** Writing – review & editing, Visualization, Validation, Software, Resources, Project administration, Methodology, Investigation, Funding acquisition, Formal analysis, Data curation, Conceptualization. **Jens Muff:** Writing – review & editing, Visualization, Validation, Supervision, Software, Resources, Project administration, Methodology, Investigation, Funding acquisition, Formal analysis, Data curation, Conceptualization.

Declaration of competing interest

The authors declare that they have no known competing financial interests or personal relationships that could have appeared to influence the work reported in this paper.

Data availability

The data that has been used is confidential.

Acknowledgments

The work was financially supported by the Danish Offshore Technology Centre as part of the research programme Produced Water Management. The authors would like to thank Benaiah Anabaraonye (DTU Offshore, Programme Manager of the research programme Produced Water Management), Simon Ivar Andersen (DTU Offshore, Research Director, Chemical Impact of Offshore Energy Production), Yanina D. Ivanova (DTU Offshore, Production Chemistry Advisor), Ole Andersen (DTU Offshore, Surface Engineer Advisor) for the continuous and insightful technical discussions during the execution of this work.

Appendix A. Supplementary data

Supplementary data to this article can be found online at https://doi.org/10.1016/j.chemosphere.2024.142439.

References

Ahmad, N.N.R., Mohammad, A.W., Mahmoudi, E., Ang, W.L., Leo, C.P., Teow, Y.H., 2022. An overview of the modification strategies in developing antifouling nanofiltration membranes. Membranes 12.
Ali, M.E.A., Wang, L., Wang, X., Feng, X., 2016. Thin film composite membranes embedded with graphene oxide for water desalination. Desalination 386, 67–76.
Amini, M., Jahanshahi, M., Rahimpour, A., 2013. Synthesis of novel thin film nanocomposite (TFN) forward osmosis membranes using functionalized multi-walled carbon nanotubes. J. Membr. Sci. 435, 233–241.
Amiri, S., Vatanpour, V., He, T., 2023. Antifouling thin-film nanocomposite NF membrane with polyvinyl alcohol-sodium alginate-graphene oxide nanocomposite hydrogel coated layer for As(III) removal. Chemosphere 322, 138159.
Bano, S., Mahmood, A., Kim, S.-J., Lee, K.-H., 2015. Graphene oxide modified polyamide nanofiltration membrane with improved flux and antifouling properties. J. Mater. Chem. A 3, 2065–2071.
Butler, E.L., Petit, C., Livingston, A.G., 2020. Poly(piperazine trimesamide) thin film nanocomposite membrane formation based on MIL-101: filler aggregation and interfacial polymerization dynamics. J. Membr. Sci. 596, 117482.
Cao, L., Zhang, Y., Ni, L., Feng, X., 2022. A novel loosely structured nanofiltration membrane bioreactor for wastewater treatment: process performance and membrane fouling. J. Membr. Sci. 644, 120128.
Cheng, X., Cai, W., Chen, X., Shi, Z., Li, J., 2019. Preparation of graphene oxide/poly (vinyl alcohol) composite membrane and pervaporation performance for ethanol dehydration. RSC Adv. 9, 15457–15465.
Chong, C.-Y., Lau, W.-J., Yusof, N., Lai, G.-S., Ismail, A.F., 2019. Roles of nanomaterial structure and surface coating on thin film nanocomposite membranes for enhanced desalination. Compos. B Eng. 160, 471–479.
Dave, H.K., Nath, K., 2016. Graphene oxide incorporated novel polyvinyl alcohol composite membrane for pervaporative recovery of acetic acid from vinegar wastewater. J. Water Proc. Eng. 14, 124–134.
Ge, R., Huo, T., Gao, Z., Li, J., Zhan, X., 2023. GO-based membranes for desalination. Membranes 13 (2), 220.
Ghosh, A.K., Hoek, E.M.V., 2009. Impacts of support membrane structure and chemistry on polyamide–polysulfone interfacial composite membranes. J. Membr. Sci. 336, 140–148.
Guo, M., Wang, S., Gu, K., Song, X., Zhou, Y., Gao, C., 2019. Gradient cross-linked structure: towards superior PVA nanofiltration membrane performance. J. Membr. Sci. 569, 83–90.
Han, Y., Xu, Z., Gao, C., 2013. Ultrathin graphene nanofiltration membrane for water purification. Adv. Funct. Mater. 23, 3693–3700.

Huang, X., Marsh, K.L., McVerry, B.T., Hoek, E.M.V., Kaner, R.B., 2016. Low-fouling antibacterial reverse osmosis membranes via surface grafting of graphene oxide. ACS Appl. Mater. Interfaces 8, 14334–14338.
Hung, W.-S., Chiao, Y.-H., Sengupta, A., Lin, Y.-W., Wickramasinghe, S.R., Hu, C.-C., Tsai, H.-A., Lee, K.-R., Lai, J.-Y., 2019. Tuning the interlayer spacing of forward osmosis membranes based on ultrathin graphene oxide to achieve desired performance. Carbon 142, 337–345.
Idris, S.N.A., Jullok, N., Lau, W.J., Ong, H.L., Dong, C.-D., 2020. Graphene oxide incorporated polysulfone substrate for flat sheet thin film nanocomposite pressure retarded osmosis membrane. Membranes 10, 416.
Igbinigun, E., Fennell, Y., Malaisamy, R., Jones, K.L., Morris, V., 2016. Graphene oxide functionalized polyethersulfone membrane to reduce organic fouling. J. Membr. Sci. 514, 518–526.
Izadmehr, N., Mansourpanah, Y., Ulbricht, M., Rahimpour, A., Omidkhah, M.R., 2020. TETA-anchored graphene oxide enhanced polyamide thin film nanofiltration membrane for water purification; performance and antifouling properties. J. Environ. Manag. 276, 111299.
Kang, Y., Obaid, M., Jang, J., Kim, I.S., 2019. Sulfonated graphene oxide incorporated thin film nanocomposite nanofiltration membrane to enhance permeation and antifouling properties. Desalination 470, 114125.
Karman, C.C., Smit, M.G., 2019. Whole effluent toxicity data and discharge volumes to assess the likelihood that environmental risks of offshore produced water discharges are adequately controlled. Integrated Environ. Assess. Manag. 15, 584–595.
Kashyap, S., Pratihar, S.K., Behera, S.K., 2016. Strong and ductile graphene oxide reinforced PVA nanocomposites. J. Alloys Compd. 684, 254–260.
Kelland, M.A., 2014. Hydrogen sulfide scavengers. In: Kelland, M.A. (Ed.), Production Chemicals for the Oil and Gas Industry. Taylor & Francis Group, CRC Press, pp. 353–368.
Khalil, A., Montesantos, N., Maschietti, M., Muff, J., 2022a. Facile fabrication of high performance nanofiltration membranes for recovery of triazine-based chemicals used for H2S scavenging. J. Environ. Chem. Eng. 10, 108735.
Khalil, H., Hegab, H.M., Nassar, L., Wadi, V.S., Naddeo, V., Yousef, A.F., Banat, F., Hasan, S.W., 2022b. Asymmetrical ultrafiltration membranes based on polylactic acid for the removal of organic substances from wastewater. J. Water Proc. Eng. 45, 102510.
Khoo, Y.S., Lau, W.J., Liang, Y.Y., Karaman, M., Gürsoy, M., Ismail, A.F., 2022. Eco-friendly surface modification approach to develop thin film nanocomposite membrane with improved desalination and antifouling properties. J. Adv. Res. 36, 39–49.
Kong, Q., Xu, H., Liu, C., Yang, G., Ding, M., Yang, W., Lin, T., Chen, W., Gray, S., Xie, Z., 2020. Fabrication of high performance TFN membrane containing NH2-SWCNTs via interfacial regulation. RSC Adv. 10, 25186–25199.
Lai, G.S., Lau, W.J., Goh, P.S., Ismail, A.F., Yusof, N., Tan, Y.H., 2016. Graphene oxide incorporated thin film nanocomposite nanofiltration membrane for enhanced salt removal performance. Desalination 387, 14–24.
Lai, G.S., Lau, W.J., Goh, P.S., Ismail, A.F., Tan, Y.H., Chong, C.Y., Krause-Rehberg, R., Awad, S., 2018. Tailor-made thin film nanocomposite membrane incorporated with graphene oxide using novel interfacial polymerization technique for enhanced water separation. Chem. Eng. J. 344, 524–534.
Lai, G.S., Lau, W.J., Goh, P.S., Tan, Y.H., Ng, B.C., Ismail, A.F., 2019. A novel interfacial polymerization approach towards synthesis of graphene oxide-incorporated thin film nanocomposite membrane with improved surface properties. Arab. J. Chem. 12, 75–87.
Lü, Z., Ding, G., Liu, M., Yu, S., Gao, C., 2023. Improved separation performance, anti-fouling property and durability of polyamide-based RO membrane by constructing a polyvinyl alcohol/polyquaternium-10 surface coating layer. Desalination 564, 116755.
Ma, X.-H., Yao, Z.-K., Yang, Z., Guo, H., Xu, Z.-L., Tang, C.Y., Elimelech, M., 2018. Nanofoaming of polyamide desalination membranes to tune permeability and selectivity. Environ. Sci. Technol. Lett. 5, 123–130.
Mansourpanah, Y., Ghanbari, A., Yazdani, H., Mohammadi, A.G., Rahimpour, A., 2021. Silver-polyamidoamine/graphene oxide thin film nanofiltration membrane with improved antifouling and antibacterial properties for water purification and desalination. Desalination 511, 115109.
Marcano, D.C., Kosynkin, D.V., Berlin, J.M., Sinitskii, A., Sun, Z., Slesarev, A., Alemany, L.B., Lu, W., Tour, J.M., 2010. Improved synthesis of graphene oxide. ACS Nano 4, 4806–4814.
Mokarizadeh, H., Moayedfard, S., Maleh, M.S., Mohamed, S.I.G.P., Nejati, S., Esfahani, M.R., 2021. The role of support layer properties on the fabrication and performance of thin-film composite membranes: the significance of selective layer-support layer connectivity. Sep. Purif. Technol. 278, 119451.
Montesantos, N., Fini, M.N., Muff, J., Maschietti, M., 2022. Proof of concept of hydrothermal oxidation for treatment of triazine-based spent and unspent H2S scavengers from offshore oil and gas production. Chem. Eng. J. 427, 131020.
Montesantos, N., Skjolding, L.M., Baun, A., Muff, J., Maschietti, M., 2023. Reducing the environmental impact of offshore H2S scavenging wastewater via hydrothermal oxidation. Water Res. 230, 119507.
Ng, Z.C., Lau, W.J., Ismail, A.F., 2020. GO/PVA-integrated TFN RO membrane: exploring the effect of orientation switching between PA and GO/PVA and evaluating the GO loading impact. Desalination 496, 114538.
Nikbakht Fini, M., Montesantos, N., Maschietti, M., Muff, J., 2021. Performance evaluation of membrane filtration for treatment of H2S scavenging wastewater from offshore oil and gas production. Sep. Purif. Technol. 277, 119641.
Niu, C., Li, X., Dai, R., Wang, Z., 2022. Artificial intelligence-incorporated membrane fouling prediction for membrane-based processes in the past 20 years: a critical review. Water Res. 216, 118299.
Poolachira, S., Velmurugan, S., 2022. Efficient removal of lead ions from aqueous solution by graphene oxide modified polyethersulfone adsorptive mixed matrix membrane. Environ. Res. 210, 112924.
Romero, I., Montero, F., Kucheryavskiy, S., Wimmer, R., Andreasen, A., Maschietti, M., 2023. Temperature- and pH-dependent kinetics of the aqueous phase hydrogen sulfide scavenging reactions with MEA-triazine. Ind. Eng. Chem. Res. 62, 8269–8280.
Shah, A.A., Cho, Y.H., Choi, H.-g., Nam, S.-E., Kim, J.F., Kim, Y., Park, Y.-I., Park, H., 2019. Facile integration of halloysite nanotubes with bioadhesive as highly permeable interlayer in forward osmosis membranes. J. Ind. Eng. Chem. 73, 276–285.
Shukla, A.K., Alam, J., Alhoshan, M., Dass, L.A., Muthumareeswaran, M.R., 2017. Development of a nanocomposite ultrafiltration membrane based on polyphenylsulfone blended with graphene oxide. Sci. Rep. 7, 41976.
Stipanicev, M., Birketveit, Ø., Kvalheim, V.H., Hoshowski, J., Lioliou, M.G., Rindalsholt, T., 2018. Multifunctional H2S scavenger and corrosion inhibitor: addressing integrity challenges and production output of the mature field. In: SPE International Oilfield Corrosion Conference and Exhibition 190911-MS.
Ugur Nigiz, F., 2020. Graphene oxide-sodium alginate membrane for seawater desalination through pervaporation. Desalination 485, 114465.
Wang, Z., Yu, H., Xia, J., Zhang, F., Li, F., Xia, Y., Li, Y., 2012. Novel GO-blended PVDF ultrafiltration membranes. Desalination 299, 50–54.
Wang, J., Wang, L., He, M., Wang, X., Lv, Y., Huang, D., Wang, J., Miao, R., Nie, L., Hao, J., Wang, J., 2022. Recent advances in thin film nanocomposite membranes containing an interlayer (TFNi): fabrication, applications, characterization and perspectives. RSC Adv. 12, 34245–34267.
Wu, X., Yang, L., Shao, W., Lu, X., Liu, X., Li, M., 2021. Fabrication of high performance TFN membrane incorporated with graphene oxide via support-free interfacial polymerization. Sci. Total Environ. 793, 148503.
Wu, H., Zhao, H., Lin, Y., Liu, X., Yao, H., Yu, L., Wang, H., Wang, X., 2022. Fabrication of polysulfone membrane with sponge-like structure by using different non-woven fabrics. Sep. Purif. Technol. 297, 121553.
Xue, S.-M., Xu, Z.-L., Tang, Y.-J., Ji, C.-H., 2016. Polypiperazine-amide nanofiltration membrane modified by different functionalized multiwalled carbon nanotubes (MWCNTs). ACS Appl. Mater. Interfaces 8, 19135–19144.
Yin, J., Zhu, G., Deng, B., 2016. Graphene oxide (GO) enhanced polyamide (PA) thin-film nanocomposite (TFN) membrane for water purification. Desalination 379, 93–101.
Zhang, Q., Zhang, C., Xu, J., Nie, Y., Li, S., Zhang, S., 2016. Effect of poly(vinyl alcohol) coating process conditions on the properties and performance of polyamide reverse osmosis membranes. Desalination 379, 42–52.
Zhao, W., Liu, H., Meng, N., Jian, M., Wang, H., Zhang, X., 2018. Graphene oxide incorporated thin film nanocomposite membrane at low concentration monomers. J. Membr. Sci. 565, 380–389.
Zhao, D.L., Feng, F., Shen, L., Huang, Z., Zhao, Q., Lin, H., Chung, T.-S., 2023. Engineering metal–organic frameworks (MOFs) based thin-film nanocomposite (TFN) membranes for molecular separation. Chem. Eng. J. 454, 140447.